energies

MDPI

Article

Coordinated State-of-Charge Balancing and Energy Management for a DC Microgrid Under Dynamic Renewable Conditions

Muhammad Sadiq [1], Saher Javaid [1,2,*], Iacovos I. Ioannou [3,4,5], Yuto Lim [1] and Yasuo Tan [1]

[1] Graduate School of Advanced Science and Technology, Japan Advanced Institute of Science and Technology, Nomi 923-1292, Ishikawa, Japan; sadiq@jaist.ac.jp (M.S.)
[2] Department of Information Engineering, Kanazawa Gakuin University, Kanazawa 920-1392, Ishikawa, Japan
[3] Department of Computer Science, University of Cyprus, 1678 Nicosia, Cyprus; ioannou.iakovos@ucy.ac.cy
[4] CYENS Centre of Excellence, 1016 Nicosia, Cyprus
[5] Department of Computer Science and Engineering, European University of Cyprus, 2404 Nicosia, Cyprus
* Correspondence: saher@jaist.ac.jp or saher@kanazawa-gu.ac.jp

Abstract

This paper presents an energy-management and state-of-charge (SoC) balancing scheme, denoted OEMSS, for a DC microgrid comprising photovoltaic generation, a fuel-cell source, two energy storage systems (ESSs), and six household loads. A demand-driven power-allocation layer first determines whether generation is sufficient, ESS support is required, or priority-based load scheduling must be activated. A supervisory balancing layer then allocates the fleet charging or discharging request by using a capacity-weighted average SoC and separate mode-dependent correction laws. The balancing command is dimensionally expressed as an energy-capacity deviation divided by the control interval and is projected onto the SoC and power limits. A Python simulation driven by recorded generation profiles is used to evaluate four seasonal operating conditions. In the tested equal-capacity case, the maximum inter-ESS SoC deviation is reduced from 18% to 4.8%, synchronization is reached within approximately 2 to 4 h, and simulated over-discharge events are avoided. The reported increase from 45% to approximately 70% is interpreted as a 25-percentage-point increase in the ESS storage contribution rate, rather than an increase in conversion efficiency. During shortage intervals, the retained priority demand is supplied, whereas satisfaction of the original uncurtailed demand is not claimed. A discrete-time Lyapunov analysis gives the nominal convergence condition $0 < \gamma_b < 2$, and the online implementation has $\mathcal{O}(J + K + H)$ time complexity. The study provides simulation evidence for a simple coordinated allocation rule; hardware performance, battery-life extension, converter-level stability, and global optimality remain to be established.

Keywords: SoC balancing; DC microgrid; adaptive control; power sharing; RES integration; power flow control; power fluctuation

Check for updates

Academic Editor: Angela Russo

Received: 19 June 2026
Revised: 24 July 2026
Accepted: 31 July 2026
Published: 4 August 2026

Copyright: © 2026 by the authors. Licensee MDPI, Basel, Switzerland. This article is an open access article distributed under the terms and conditions of the Creative Commons Attribution (CC BY) license.

1. Introduction

Structural changes that involve both power generation and transmission systems over the last couple of years have resulted from energy security and climate change concerns, as well as the need for reliability. Adaptive changes in power generation, such as renewable energy sources (RESs) including solar photovoltaic (PV) systems and wind turbines, exhibit quite different inertial and dynamic characteristics compared to synchronous machine-based power generation. The future of decentralized power systems, including microgrids and nanogrids, is promising [1]. Decentralized systems offer reliable, local control and

reduced reliance on centralized infrastructure. Microgrids and nanogrids, integrated with RES and ESS, are key for managing energy demand and ensuring reliability during extreme weather events. These systems also support the growing use of distributed solar panels, batteries, and electric vehicles, paving the way for a more flexible and efficient energy infrastructure. One of the biggest differences is the fluctuating and unpredictable power generation behavior. Conventional generators are directly synchronized through the grid, while in contrast, renewable energy sources cannot connect directly with the power grid but instead use an additional power electronic converter to connect the RES to AC systems [2]. This makes the interaction very different from that of other grid-connected systems.

On the other hand, with the advent of smart homes, intelligent devices, and advancements in home automation, human lifestyles have become increasingly reliant on energy-powered equipment. This has led to a rapid rise in energy demand. In DPN, power consumption patterns are highly unpredictable and fluctuate based on user behavior. Coupled with the intermittency of power generation from RES, effective power management is essential to balance supply and demand. While RES offers significant benefits, its integration poses challenges. ESS emerges as a leading solution to mitigate fluctuations in generation and consumption [3], facilitating smoother adoption of RES. ESS can store excess power during peak periods of power generation and release it during low periods or in the absence of power generation. However, ESS faces several challenges such as economic cost, limited energy density, and degradation over time.

In DPN, several ESS units are deployed to store surplus energy generated from RES and to provide energy to various loads during peak demand. However, multiple ESS units introduce challenges in harmonious operation and optimization of energy utilization. Each ESS may experience different initial conditions and charge/discharge rates due to varying user behavior or generation profiles. This usually results in asynchronous SoC, which increases the risk of overcharging or deep discharging, potentially affecting the performance and lifetime of the ESS. To address this problem [4], SoC synchronization ensures consistent energy distribution and prevents imbalances that can degrade ESS performance or reduce system efficiency. In order to maintain stability and prolong the life of the batteries, advanced control strategies, algorithms, and communication between ESS units should be implemented. These methods synchronize the SoC across the network, allowing for efficient energy sharing, better handling of loads, and seamless integration with RES. This kind of synchronization is very important for ensuring reliability within DPN, nanogrids, and microgrids.

2. Literature Review

Smart Energy Management Systems (SEMSs) have received considerable attention in residential research because they support more effective coordination of household energy use. Interest in DC power networks and microgrids has also increased as emissions requirements have become stricter and fuel-efficiency objectives have grown. In shipboard applications, this development is closely associated with the transition toward All-Electric Ships (AESs), for which dependable DC-microgrid power-flow calculations are required. The method reported in [2] evaluates a representative shipboard DC network by determining node voltages, branch currents and equipment-loop operating states. These quantities provide the steady-state and quasi-steady-state information needed for subsequent system design, controller development, and validation.

System-level surveys provide a wider view of microgrid (MG) technology and its interacting subsystems. The review in [5] organizes prior work across component design, renewable generation, storage, load categories, communication and control infrastructure, energy-management methods, operating modes, and interconnected MG architectures. It

further identifies intermittent renewable energy resources (RERs) and active loads as sources of stability, power-quality, and cyber–physical challenges when renewable and storage penetration increases. These observations establish the cross-disciplinary constraints that must be considered when MG power-flow and control methods are designed. At the community level, aggregator-coordinated groups of DC nanogrids have been examined as a means of forming renewable-energy communities. The approach in [6,7] numerically assesses residential nanogrids that use DC Bus Signaling to communicate local voltage information to an aggregator. This exchange allows the regulation capacity to be adjusted and the local PV and battery resources to be coordinated. The reported results indicate that lightweight signaling can support scalable participation in services that extend beyond an individual nanogrid.

Reference [8] structures an MG into three modular layers and assigns continuous power-management responsibility to the Basic DC MG Model in Layer 1. Alternative energy-management objectives can then be implemented by changing the voltage-regulation priority assigned to each device, including reduced battery-capacity requirements or lower dependence on the AC grid. A related community-energy configuration is examined in [9], where several DC nanogrids are coordinated through an aggregator. Each nanogrid applies DC Bus Signaling (DBS) to modify its local power flow in accordance with aggregator requests while retaining the ability to operate independently when no service is requested. Earlier studies have mainly examined power-flow control during periods in which renewable generation and consumption are both high. The home energy-management approach in [10] applies a balancing-power negotiation mechanism to coordinate power allocation and shift flexible loads. This line of work demonstrates the importance of demand–response and automated demand–response functions for maintaining agreement between available generation and time-varying consumption. On the other hand, regarding the efficient usage of ESS in a safe and reliable system, ref. [11] develops safety conditions for ESS for safe usage, and also introduces the optimal sizing of ESS to integrate the RES in the power system. In [12], a consensus-based distributed cooperative control strategy is proposed to simultaneously alleviate voltage fluctuations, prolong battery lifespan, and enhance battery efficiency. In [13], power balancing strategies for resilient operation of BESS using a double-star chopper cell (DSCC) topology-based MMC under asymmetric AC grid voltage scenarios are proposed. Similarly, ref. [14] presents a novel droop-based distributed SoC balancing control scheme designed to eliminate SoC discrepancies among distributed energy storage units (DESUs) of varying capacities, thereby supporting system scalability and uniform performance. Furthermore, ref. [15] introduces a method to improve the equalization rate of battery state of charge (SoC) among distributed energy storage subsystems in DC microgrids, addressing issues of overcharging and over-discharging caused by SoC imbalances.

SoC balancing is a critical aspect of maintaining efficiency and extending the lifespan of energy storage systems (ESS) in both stand-alone and microgrid configurations. Various approaches have been explored to achieve SoC equalization across heterogeneous or distributed cells. In [16], an active SoC balancing scheme for multi-chemistry or second-life cells was introduced, employing a reduced number of converters to lower system cost while maintaining balancing performance. The study proposed two converter-based configurations, namely, direct cell-to-cell and time-multiplexed balancing via an auxiliary low-voltage bus, demonstrating improved efficiency compared to traditional single-converter or fully distributed solutions. Similarly, the work in [17] combined a Virtual DC Motor (VDCM) control strategy with a dynamic consensus algorithm to achieve SoC consistency in DC microgrids. The proposed control layer enhanced DC bus voltage stability and improved energy utilization across distributed storage units. Intelligent control has also been explored for SoC regulation. In [18], a Q-learning-based reinforcement learning (RL) algorithm

was implemented for SoC balancing in a Battery Modular Multilevel Management (BM3) converter topology. The results highlighted the potential of RL for adaptive balancing across multiple battery modules, although scalability remained a challenge. Meanwhile, the review in [19] analyzed Battery Power Module (BPM) architectures where each cell is decoupled via a low-power DC-to-DC converter. The study compared multiple converter types and control algorithms, emphasizing the trade-off between SoC estimation accuracy, control complexity, and sensor requirements.

Machine learning-based balancing techniques have also gained traction. A stacking ensemble learning approach for SoC estimation and control of EV charging stations was proposed in [20], leveraging Kalman filtering to dynamically adapt to fluctuating charging demands. This approach achieved improved SoC estimation accuracy and reduced network loss rates, demonstrating strong adaptability under variable load conditions. For distributed ESS and microgrid applications, several droop-based control methods have been proposed to address SoC imbalance. In [21], an adaptive droop control strategy incorporating dynamic correction coefficients was introduced to coordinate power sharing among distributed storage units, ensuring stable operation and extended battery life. Similarly, ref. [22] proposed a droop-based control with an acceleration coefficient to expedite SoC equalization and maintain optimal power quality in distributed systems. Furthermore, ref. [23] presented an improved P–f droop control scheme that incorporated an exponential equalization factor to regulate inverter output power, achieving SoC balancing among BESS units with different capacities. The authors also analyzed the system's small-signal stability and identified design guidelines for tuning the acceleration factor. Collectively, these studies show that proportional SoC feedback, adaptive droop, and consensus coordination are established principles. The contribution of the present work is therefore not attributed to the general use of an SoC deviation term. Instead, the proposed contribution is the specific supervisory integration of demand-driven allocation, a capacity-weighted fleet reference, mode-dependent charging and discharging corrections, feasibility projection, priority-load scheduling, and a storage contribution indicator. Table 1 makes this distinction explicit. "NR" denotes a capability or result that was not reported in the cited study and does not necessarily indicate that the capability is impossible.

Table 1. Positioning of OEMSS relative to representative SoC balancing methods.

Panel A: Architecture and Supported Operating Features					
Method	**Control and Communication**	**Unequal Capacity**	**Renewable and Load Variability**	**Voltage Role**	**Load Priority**
Distributed cooperative control [12]	Distributed consensus and information exchange	Included in dispatch formulation	Limited operating cases	Secondary voltage and economic coordination	No
VDCM with dynamic consensus [17]	Distributed VDCM with consensus exchange	NR	Disturbance scenarios	Explicit DC-bus regulation	No
Droop-based distributed balancing [14]	Distributed droop with sparse communication links	Considered	NR	Droop-based voltage and power sharing	No
Equalization-rate improvement [15]	Distributed droop-type control	NR	NR	DC-bus-oriented droop regulation	No
Adaptive droop with correction coefficients [21]	Distributed droop with local SoC correction	NR	Variable operating conditions	Droop-based voltage and power sharing	No
Droop with acceleration coefficient [22]	Decentralized droop control	NR	Selected load cases	Power-quality-oriented droop	No

Table 1. *Cont.*

Panel A: Architecture and Supported Operating Features					
Method	**Control and Communication**	**Unequal Capacity**	**Renewable and Load Variability**	**Voltage Role**	**Load Priority**
Multi-ESS acceleration-factor droop [23]	Decentralized P–f droop	Considered	Selected operating cases	Small-signal stability analyzed	No
OEMSS in this study	Central supervisory SoC exchange coordinated with DDPA	Supported analytically; equal-capacity case tested	Four seasonal profiles and household-load variation	Supervisory guard only; no converter-level regulation claim	Yes, through DDPA
Panel B: Objective, Computational Burden and Evidence					
Method	**Primary Objective**	**Online Burden**	**Validation**	**Reported SoC Outcome**	
Distributed cooperative control [12]	SoC balance and economic dispatch	Iterative neighbor updates	Simulation	Convergence reported	
VDCM with dynamic consensus [17]	SoC consistency and voltage support	Consensus and VDCM states	MATLAB simulation	Convergence reported	
Droop-based distributed balancing [14]	SoC equalization across units of varying capacity	Local algebraic update	Simulation	Equalization with scalability reported	
Equalization-rate improvement [15]	Faster SoC equalization among subsystems	Local algebraic update	Simulation	Improved equalization rate reported	
Adaptive droop with correction coefficients [21]	SoC balance and power sharing	Local algebraic update	Simulation	Improved equalization reported	
Droop with acceleration coefficient [22]	Faster SoC equalization	Local algebraic update	Simulation	Accelerated convergence reported	
Multi-ESS acceleration-factor droop [23]	SoC balance with stability-aware gain selection	Local algebraic update	Simulation	Convergence and gain guidance reported	
OEMSS in this study	Demand allocation with mode-dependent SoC redistribution	$\mathcal{O}(J+K+H)$	Python simulation with recorded source profiles	18% to 4.8%; 2 to 4 h in tested cases	

The table also shows the limitations of the current evidence. OEMSS requires the supervisory controller to receive the SoC and capacity of each ESS, whereas several droop-based methods use only local measurements. Unequal capacities are handled by the capacity-weighted equations, but only the equal-capacity two-ESS case is evaluated. The voltage guard prevents the supervisory command from opposing the faster bus controller; it is not a substitute for converter-level voltage regulation or small-signal validation. No hardware-in-the-loop or physical battery experiment is reported.

3. Research Motivation and Gap

The cited literature already contains proportional SoC-sharing, adaptive-droop, and consensus-based balancing laws [12,14,15,17,21–23]. Accordingly, this study does not claim that power adjustment according to SoC deviation is new by itself. The unresolved design question considered here is how a lightweight SoC balancing rule can be placed inside a demand-oriented energy-management sequence that also decides when storage support or priority-load scheduling is required. As illustrated in Figure 1, uncoordinated ESS operation can produce increasing SoC differences among storage units. The proposed

balancing mechanism adjusts their charging and discharging contributions to reduce this deviation while maintaining the defined SoC limits.

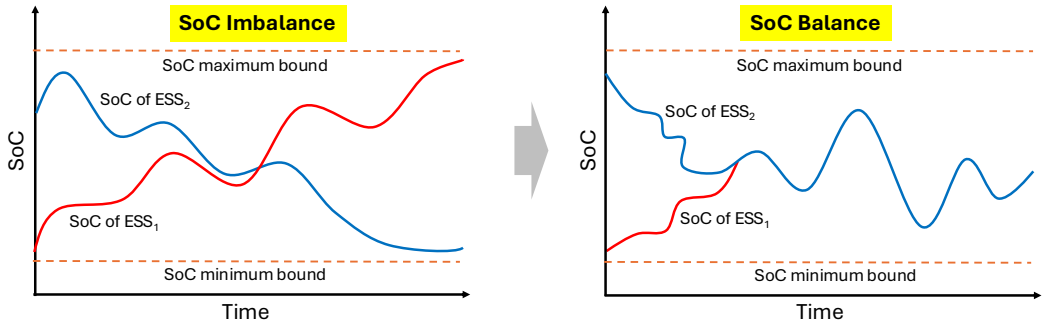


Figure 1. Illustration of SoC balancing concept.

The mathematical distinction is as follows. DDPA produces a nonnegative fleet charging request or a nonnegative fleet discharging request from the generation–demand imbalance. OEMSS forms a capacity-weighted average SoC, distributes the common request in proportion to ESS energy capacity, applies a mode-dependent correction that decreases charging or increases discharging for an above-average ESS, and projects the resulting commands onto the power and SoC constraints. The same rule is applied with the opposite physical effect to a below-average ESS. This formulation explicitly separates charging and discharging and remains dimensionally consistent through the factor C_{ES_h}/T_s.

The study also reports the quantity historically denoted ESS_{UR}. Because this ratio measures cumulative ESS discharge relative to cumulative demand, it is interpreted here as a storage contribution rate. It is not a round-trip efficiency, converter efficiency, battery-health metric, or direct measure of lifetime extension. The acronym OEMSS is retained for continuity; however, no proof of global optimality is claimed.

The contributions evaluated in this work are therefore limited to three points:

1. A two-layer integration of demand-driven allocation and multiple-ESS SoC redistribution;
2. Dimensionally consistent and mode-dependent charging and discharging allocation rules with a capacity-weighted SoC reference and feasibility projection;
3. Simulation-based assessment under four recorded seasonal generation profiles, together with explicit reporting of SoC convergence and storage contribution.

The present evidence is obtained from a Python supervisory energy-flow simulation that uses recorded generation profiles. It is not an experimental or hardware-in-the-loop validation. Battery chemistry, switching behavior, electrochemical aging, and converter inner-loop dynamics are outside the present model and are identified as limitations rather than inferred benefits.

4. System Model and Control Framework

This section presents the system model of the microgrid, as illustrated in Figure 2. The system model mainly consists of the PV Energy Generation (EGs) system, the Energy Storage (ESs) system, and the Energy Loads (ELs). In the DPN, the system formalizes EGs, ELs, and ESs. Here, $\mathcal{J}$, $\mathcal{K}$, and $\mathcal{H}$ are the sets of EGs, ELs, and ESs. We denote $EG_j^f(t)$ as a set of fluctuating EGs at time t, where $j \in J = \{1, 2, \ldots, J\}$ and J is the total number of EGs. $EL_k^f(t)$ is a set of fluctuating ELs at time t, where $k \in K = \{1, 2, \ldots, K\}$ and K is the total number of ELs. $ES_h^c(t)$ is a set of controllable ESs at time t, where $h \in H = \{1, 2, \ldots, H\}$ and H is the total number of ESs.

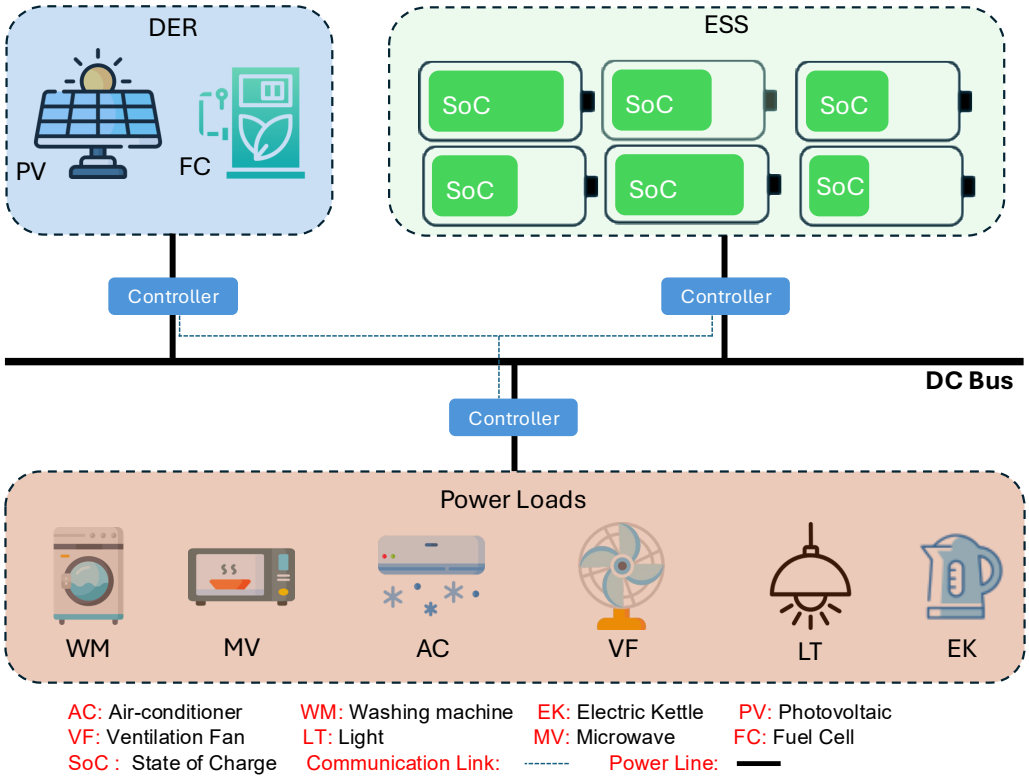


Figure 2. Overall system configuration and control architecture of the DC microgrid.

These three components are mainly connected through the DC bus for power flow between them. $\mathcal{E}_{\mathrm{EG}}$ is denoted as the energy generated from the EGs, which flows from EGs toward the ESs and ELs. Stored energy is denoted as $\mathcal{E}_{\mathrm{ES}}$, which can flow from the EGs to the ESs or from ESs to the ELs. Load energy, denoted as $\mathcal{E}_{\mathrm{EL}}$, flows from EGs and ESs toward the ELs. The energy balance relationship of the DC microgrid can be expressed as in (1):

$$\mathcal{E}_{\mathrm{EG}} = \mathcal{E}_{\mathrm{EL}} + \mathcal{E}_{\mathrm{ES}} + \mathcal{E}_{\mathrm{loss}} \tag{1}$$

where $\mathcal{E}_{\mathrm{EG}}$ and $\mathcal{E}_{\mathrm{EL}}$ can be computed as

$$\mathcal{E}_{\mathrm{EG}}(t) = \int_0^t \left(\sum_{j \in J} EG_j(\tau) \right) d\tau \tag{2}$$

$$\mathcal{E}_{\mathrm{EL}}(t) = \int_0^t \left(\sum_{k \in K} EL_k(\tau) \right) d\tau \tag{3}$$

where $\mathcal{E}_{\mathrm{ES}}$ represents the stored energy of the ESs. It can be computed as

$$\mathcal{E}_{\mathrm{ES}_h}(t) = \mathcal{E}^{ini}_{\mathrm{ES}_h} + \mathcal{E}^{in}_{\mathrm{ES}_h}(t) - \mathcal{E}^{out}_{\mathrm{ES}_h}(t) \tag{4}$$

where $\mathcal{E}^{ini}_{\mathrm{ES}_h}$ is the initial energy of the h-th ES. It can be computed as

$$\mathcal{E}^{ini}_{\mathrm{ES}_h} = (SoC^{ini}_h - SoC^{min}_h) \times C_{ES_h} \tag{5}$$

where SoC^{ini}_h represents the initial state of charge of the ESs, SoC^{min}_h represents the minimum state of charge, and C_{ES_h} denotes the rated energy capacity of the h-th ES.

$\mathcal{E}^{in}_{\mathrm{ES}_h}$ is the charging energy that is computed using the charging power $\mathcal{P}^{in}_{\mathrm{ES}_h}$ and the charging efficiency η_c of the ESs, and $\mathcal{E}^{out}_{\mathrm{ES}_h}$ is the discharging energy that is computed using

the discharge power $\mathcal{P}^{out}_{\mathrm{ES}_h}$ and the discharging efficiency η_d of the ESs. These are calculated from time 0 to time t as

$$\mathcal{E}^{in}_{\mathrm{ES}_h}(t) = \eta_c \cdot \int_0^t \mathcal{P}^{in}_{\mathrm{ES}_h}(\tau)\, d\tau \tag{6}$$

$$\mathcal{E}^{out}_{\mathrm{ES}_h}(t) = \frac{1}{\eta_d} \cdot \int_0^t \mathcal{P}^{out}_{\mathrm{ES}_h}(\tau)\, d\tau \tag{7}$$

Here, the charging energy in (7) accounts for the fact that the ESS must withdraw more energy from the battery than is delivered to the load due to discharging losses.

Energy Storage Constraints

The state of charge (SoC) of the ESs can be computed as

$$SoC_h(t) = SoC^{ini}_h + \frac{\mathcal{E}^{in}_{\mathrm{ES}_h}(t)}{C_{ES_h}} - \frac{\mathcal{E}^{out}_{\mathrm{ES}_h}(t)}{C_{ES_h}} \tag{8}$$

The SoC of the energy storage units (ESs) must remain within the specified operating ranges to prevent overcharging and over-discharging, as expressed in (9). We denote the minimum state of charge as $\mathrm{SoC}^{\min}$ and the maximum state of charge as $\mathrm{SoC}^{\max}$:

$$SoC^{min}_h \le SoC_h(t) \le SoC^{max}_h \tag{9}$$

The charging power $\mathcal{P}^{in}_{\mathrm{ES}_h}$ to the ESs and the discharging power $\mathcal{P}^{out}_{\mathrm{ES}_h}$ from the ESs should remain within the bounds of the maximum and minimum limitations as given in (10) and (11):

$$\mathcal{P}^{in,min}_{\mathrm{ES}_h} \le \mathcal{P}^{in}_{\mathrm{ES}_h}(t) \le \mathcal{P}^{in,max}_{\mathrm{ES}_h} \tag{10}$$

$$\mathcal{P}^{out,min}_{\mathrm{ES}_h} \le \mathcal{P}^{out}_{\mathrm{ES}_h}(t) \le \mathcal{P}^{out,max}_{\mathrm{ES}_h} \tag{11}$$

5. Energy-Management and SoC Balancing Scheme (OEMSS)

The OEMSS is a supervisory rule-based scheme that coordinates the ESS fleet after DDPA determines the demand-management operating state. The term "optimal" is retained as part of the submitted acronym and does not denote a global optimum of a formally solved optimization problem. At sampling instant k, let $P^{orig}_L[k]$ be the original aggregate demand and let $P^{srv}_L[k] \le P^{orig}_L[k]$ be the demand retained after priority scheduling. The fleet charging and discharging requests are defined separately as

$$P^{in}_{ES}[k] = \max(0, P_G[k] - P^{srv}_L[k]), \tag{12}$$

$$P^{out}_{ES}[k] = \max(0, P^{srv}_L[k] - P_G[k]), \tag{13}$$

so that charging and discharging are not requested simultaneously.

For H storage units, the capacity-weighted average SoC and the individual deviation are

$$\overline{SoC}_C[k] = \frac{\sum_{i=1}^{H} C_{ES_i} SoC_i[k]}{\sum_{i=1}^{H} C_{ES_i}}, \tag{14}$$

$$e_h[k] = SoC_h[k] - \overline{SoC}_C[k]. \tag{15}$$

The common capacity share is $\alpha_h = C_{ES_h} / \sum_{i=1}^{H} C_{ES_i}$. Let T_s be expressed in hours, let C_{ES_h} be expressed in watt-hours, and let γ_b be a dimensionless balancing coefficient. The factor C_{ES_h}/T_s therefore has units of watts. The unconstrained charging command is

$$\widetilde{P}^{in}_{ES_h}[k] = \alpha_h P^{in}_{ES}[k] - \frac{\gamma_b C_{ES_h}}{\eta_c T_s} e_h[k], \tag{16}$$

and the unconstrained discharging command is

$$\widetilde{P}^{out}_{ES_h}[k] = \alpha_h P^{out}_{ES}[k] + \frac{\eta_d \gamma_b C_{ES_h}}{T_s} e_h[k]. \tag{17}$$

Thus, an above-average ESS receives less charging power in (16) and more discharging power in (17). A below-average ESS receives the opposite correction. Since $\sum_h C_{ES_h} e_h = 0$, the unconstrained balancing corrections sum to zero for common efficiencies and therefore redistribute rather than create fleet power.

The physically applied commands are obtained by projection:

$$\begin{aligned} P^{in}_{ES_h}[k] &= \Pi_{\Omega^{in}_h[k]}\Big(\widetilde{P}^{in}_{ES_h}[k]\Big), \\ P^{out}_{ES_h}[k] &= \Pi_{\Omega^{out}_h[k]}\Big(\widetilde{P}^{out}_{ES_h}[k]\Big). \end{aligned} \tag{18}$$

The feasible sets Ω^{in}_h and Ω^{out}_h enforce nonnegative commands, rated charging and discharging limits, SoC bounds, and any command-ramp restriction. If projection creates a residual fleet–power mismatch, the residual is redistributed among the remaining unconstrained units in proportion to their available headroom. The charging and discharging ratios are consequently defined separately as

$$Ratio^{c}_{ES_h}[k] = \frac{P^{in}_{ES_h}[k]}{P^{in}_{ES}[k]}, \qquad Ratio^{d}_{ES_h}[k] = \frac{P^{out}_{ES_h}[k]}{P^{out}_{ES}[k]}, \tag{19}$$

when the corresponding denominator is nonzero and are set to zero otherwise.

5.1. Stability and Gain Selection of the Supervisory Balancing Rule

The convergence statement concerns the supervisory SoC balancing dynamics and not the switching-converter voltage loop. In the unsaturated equal-efficiency case, substitution of (16) or (17) into the sampled SoC equation gives the same deviation dynamics in either operating mode:

$$\mathbf{e}[k+1] = (1-\gamma_b)\mathbf{e}[k] + \mathbf{w}[k], \tag{20}$$

where $\mathbf{w}[k]$ collects bounded measurement and tracking disturbances after removal of their capacity-weighted common component. For the nominal case $\mathbf{w}[k] = \mathbf{0}$, the Lyapunov function $V[k] = \frac{1}{2}\mathbf{e}^{\mathsf{T}}[k]\mathbf{e}[k]$ yields

$$\Delta V[k] = -\frac{1}{2}\gamma_b(2-\gamma_b)\|\mathbf{e}[k]\|_2^2. \tag{21}$$

Therefore, nominal asymptotic synchronization is obtained for

$$0 < \gamma_b < 2, \tag{22}$$

while $0 < \gamma_b \leq 1$ produces non-alternating error decay. Under $\|\mathbf{w}[k]\|_2 \leq \bar{w}$, the error satisfies

$$\|\mathbf{e}[k]\|_2 \leq |1-\gamma_b|^k \|\mathbf{e}[0]\|_2 + \frac{1-|1-\gamma_b|^k}{1-|1-\gamma_b|}\bar{w}. \tag{23}$$

The proof does not cover intervals in which several ESS commands are simultaneously saturated. During such intervals, feasibility is preserved by projection and residual redistribution, but the nominal convergence rate is not guaranteed. The balancing update is suspended when $|V_{dc} - V^{ref}_{dc}| > \Delta V_{guard}$ so that the converter-level voltage controller is given priority. This guard is a supervisory safeguard and does not constitute a converter small-signal stability result.

5.2. ESS Storage Contribution Rate

Figure 3 illustrates the purpose of limiting the ESS storage contribution rate. In conventional operation, load demand may depend heavily on ESS discharge, with the ESS supplying 90% or more of the required power. In the proposed OEMSS, the ESS contribution is limited to 70%, while the remaining demand is supplied by available generation. This limit reduces excessive dependence on ESS discharge and preserves stored energy for subsequent demand periods. The quantity retained from the original formulation is denoted ESS_{UR} for traceability with the figures, but it is interpreted as a storage contribution rate:

$$ESS_{UR}[N] = \frac{\sum_{k=0}^{N} P_{ES}^{out}[k]T_s}{\sum_{k=0}^{N} P_L^{orig}[k]T_s} \times 100\%. \tag{24}$$

The numerator is cumulative energy discharged by the ESS fleet and the denominator is cumulative original load energy over the same horizon. The metric therefore indicates the fraction of original demand energy associated with ESS discharge. It does not measure charging efficiency, discharging efficiency, round-trip efficiency, conversion loss, battery degradation, or avoided lifetime consumption. An increase from 45% to 70% is consequently reported as a 25-percentage-point increase in storage contribution and not as a 25% efficiency improvement. A higher value is not intrinsically better because excessive storage contribution may increase cycling; it is interpreted only together with the SoC and power constraints.

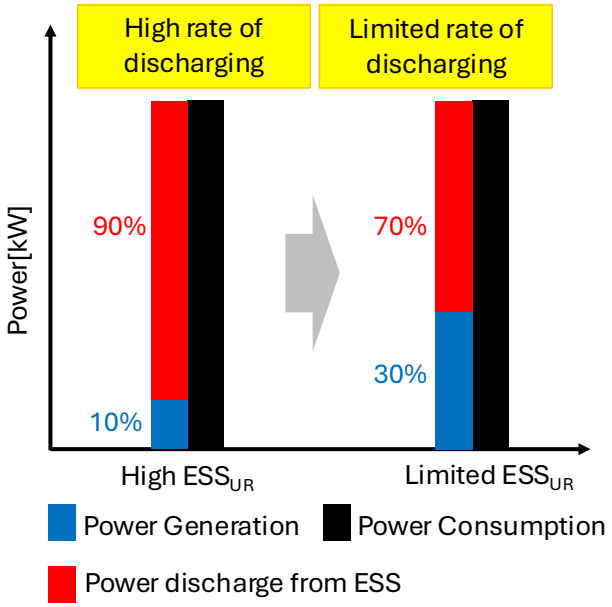


Figure 3. Concept of the ESS storage contribution rate (the legacy plot label uses "utilization").

To distinguish demand service from load prioritization, the original-demand service ratio and curtailed energy are defined as

$$DSR = \frac{\sum_{k=0}^{N} P_L^{srv}[k]T_s}{\sum_{k=0}^{N} P_L^{orig}[k]T_s} \times 100\%, \qquad E_{curt} = \sum_{k=0}^{N} \left(P_L^{orig}[k] - P_L^{srv}[k] \right) T_s. \tag{25}$$

When priority scheduling is inactive, $P_L^{srv} = P_L^{orig}$ and $DSR = 100\%$. When low-priority demand is removed, the retained priority demand may be fully supplied even though $DSR < 100\%$. These two statements are kept separate throughout the results.

6. Proposed Control Algorithms

The energy-management framework is implemented through two coordinated algorithms: OEMSS (Algorithm 1) and DDPA (Algorithm 2). DDPA selects the demand supplied at each interval and determines whether a fleet charging or discharging request exists. OEMSS then redistributes that request among the ESS units. The algorithms do not solve a global mathematical optimization problem and no global optimality claim is made.

Algorithm 1 Coordinated energy-management and SoC balancing scheme (OEMSS)

Input: P_G, P_L^{orig}, SoC_h, C_{ES_h}, power limits, T_s, γ_b, and V_{dc}
Output: P_L^{srv}, $P_{ES_h}^{in}$, $P_{ES_h}^{out}$, DSR, and ESS_{UR}
for each sampling instant k **do**
    Apply DDPA to obtain $P_L^{srv}[k] \leq P_L^{orig}[k]$
    Compute $P_{ES}^{in}[k]$ and $P_{ES}^{out}[k]$ from Equations (12) and (13)
    Compute $\overline{SoC}_C[k]$ and $e_h[k]$ for all ESS units
    if $P_{ES}^{in}[k] > 0$ **then**
        Compute the charging commands using Equation (16)
    else if $P_{ES}^{out}[k] > 0$ **then**
        Compute the discharging commands using Equation (17)
    else
        Set all ESS power commands to zero
    Project commands onto SoC, power, and ramp constraints
    Redistribute any residual request among ESS units with available headroom
    if $|V_{dc} - V_{dc}^{ref}| > \Delta V_{guard}$ **then**
        Suspend the SoC correction and retain the feasible common DDPA allocation
    Update SoC, ESS_{UR}, DSR, and E_{curt}

Algorithm 2 Demand-Driven Power Allocation (DDPA) Algorithm

Initialize: Power sources (PV, PES), loads (PL), storage (SoCES)
$P_{out} \leftarrow (P_{PV} + P_{ES}) - P_L$
Loop:
if $P_{supply} > 0$ **then**
    if $P_{ES} > P_L$ **then**
        if $P_{supply} > P_L$ **then**
            Supply fully meets load demand
        else if $P_{supply} + P_{ES} > P_L$ **then**
            Supply and storage together meet load
        else
            Go to prioritized load scheduling
            $P_L \leftarrow$ prioritized load
    else
        Go to prioritized load scheduling
        $P_L \leftarrow$ prioritized load
else
    Check for Energy Storage (ES) support
If charging condition:
Charge the ES
If discharging condition:
Discharge the ES
Repeat loop or exit as needed

6.1. Demand-Driven Power Allocation (DDPA)

The Demand-Driven Power Allocation (DDPA) algorithm serves as the primary decision-making layer for real-time power allocation within the microgrid. The objec-

tive of DDPA is to use available generation and storage while explicitly distinguishing original demand from the demand retained after priority scheduling.

At each control interval, the algorithm evaluates the available generation power and the total load demand to determine the system operating condition. When generation is sufficient to meet the demand, the system operates under normal supply conditions and excess energy can be directed toward energy storage. In situations where generation alone is insufficient, the algorithm evaluates the contribution of the ESS to support the load demand. If the combined generation and storage power remain inadequate, prioritized load scheduling is activated, allowing essential loads to be maintained while non-critical loads are temporarily reduced or disconnected.

DDPA therefore transitions between direct generation supply, storage-assisted supply, and prioritized load scheduling. In the third state, only the retained priority demand is claimed to be supplied; the curtailed part of the original profile is quantified by Equation (25).

6.2. Coordinated Energy-Management and SoC Balancing Scheme (OEMSS)

OEMSS introduces supervisory coordination of multiple ESS units. Its evaluated contribution is the integration of mode-dependent SoC redistribution with the fleet power request generated by DDPA.

OEMSS evaluates a capacity-weighted average SoC and applies separate charging and discharging laws. The analytical formulation permits unequal energy capacities, although the reported simulation uses two equal-capacity units. Battery degradation is not modeled and lifetime extension is therefore treated as an anticipated benefit rather than a verified outcome.

The reported ESS_{UR} value is a descriptive storage contribution rate. It is not used as a conversion-efficiency measure and does not by itself demonstrate reduced degradation or longer battery life.

The OEMSS algorithm operates in coordination with DDPA, where DDPA determines the required system-level power allocation and OEMSS refines the allocation at the storage level through mode-dependent SoC redistribution. The combined strategy coordinates the demand-management state and the ESS allocation. Its demonstrated outcome is reduced SoC divergence in the tested simulation profiles.

6.3. Computational Complexity and Real-Time Implementation

The computational requirements of the two coordinated algorithms are summarized in Table 2. DDPA requires the aggregation of J generation values and K load values followed by a fixed number of logical comparisons. Its time complexity is therefore $\mathcal{O}(J+K)$. OEMSS computes one capacity-weighted average followed by one deviation, balancing command and feasibility projection for each of the H ESS units. Its time complexity is $\mathcal{O}(H)$ and its working memory requirement is $\mathcal{O}(H)$. The cumulative storage-contribution and demand-service metrics are updated recursively and therefore require constant time and memory per sampling interval. The overall framework has $\mathcal{O}(J+K+H)$ time complexity and $\mathcal{O}(H)$ auxiliary memory complexity.

No matrix inversion, iterative numerical optimization or learned-model inference is required during an online update. For the evaluated configuration with two generators, six loads and two ESS units, the execution consists of short scalar loops and conditional branches. This structure is suitable in principle for low-cost microcontrollers used in nanogrid and microgrid controllers. Fixed-point arithmetic can be used after the SoC and power variables are scaled, while reciprocal capacities and gain products can be precomputed to reduce division operations. The energy-management task should be

scheduled below the bandwidth of the converter-level voltage and current controllers. Target-specific verification remains necessary because the worst-case execution time, memory use, and interrupt latency depend on the selected microcontroller, compiler, and communication interface.

Table 2. Computational requirements per energy-management update.

Operation	Time	Memory
Generation and load aggregation in DDPA	$\mathcal{O}(J+K)$	$\mathcal{O}(1)$
SoC averaging, balancing, and command projection in OEMSS	$\mathcal{O}(H)$	$\mathcal{O}(H)$
Recursive storage-contribution and demand-service updates	$\mathcal{O}(1)$	$\mathcal{O}(1)$
Combined DDPA and OEMSS update	$\mathcal{O}(J+K+H)$	$\mathcal{O}(H)$

7. Simulation

This section describes the Python-based supervisory energy-flow simulation. The evaluation is entirely software-based and does not include a physical controller or a hardware-in-the-loop platform. The DPN model contains Energy Generation units (EGs), Energy Loads (ELs) and Energy Storage units (ESs). The generation subsystem comprises a Photovoltaic Cell (PV) and a Fuel Cell (FC). The load subsystem includes an Air Conditioner (AC), Washing Machine (WM), Ventilation Fan (VF), Light (LT), Electric Kettle (EK) and Microwave (MV), whereas the storage subsystem contains ES1 and ES2. Recorded FC and PV profiles from the *i*House setup are supplied as exogenous inputs to the Python simulation; only the supervisory controller is assessed. The FC profile follows the ENE-FARM operating framework [24]. It is enabled from 00:00 to 05:00 and from 16:00 to 23:59 in every seasonal case to improve source availability. Seasonal PV variability is represented by measured profiles for 11 January, 3 April, 14 June, and 17 October, corresponding to winter, spring, summer, and autumn, respectively.

The household-load model uses six appliances selected to represent common residential demand in a microgrid. Table 3 reports their hourly activation states over a complete day and therefore shows how aggregate demand changes with time. The Air Conditioner (AC) remains active for 21 h in the adopted profile because indoor temperature control constitutes the dominant continuous load. The remaining appliances are assigned shorter operating windows that reproduce typical daily-use patterns. Their season-dependent power ratings are provided in Table 4. Table 5 then summarizes the assumptions and limits of the supervisory model. ES1 and ES2 are represented through aggregate energy-balance equations; electrochemical battery behavior and converter switching are not simulated, so unsupported device parameters are intentionally omitted. Both units have equal capacity in the evaluated case, although the mathematical formulation permits unequal capacities. The reported value of approximately 70% is an outcome of the simulated storage contribution and is not imposed as a controller reference.

Table 3. Daily activity schedule of home appliances.

Device	Active Time Periods (Hours)
AC	01:00 to 06:00, 08:00 to 24:00
WM	08:00 to 09:00, 12:00 to 13:00, 16:00 to 17:00, 22:00 to 23:00
EK	05:00 to 05:10, 07:30 to 07:40, 08:30 to 08:40, 14:00 to 14:10, 17:30 to 17:40, 19:30 to 19:40, 21:00 to 21:10, 22:00 to 22:10
LT	05:00 to 06:00, 07:00 to 09:00, 13:00 to 14:00, 15:00 to 16:00, 17:00 to 23:00
VF	07:30 to 08:30, 13:30 to 14:00, 17:00 to 18:00, 23:00 to 23:30
MV	06:10 to 06:30, 07:15 to 07:25, 08:30 to 08:45, 09:00 to 09:15, 13:30 to 13:45, 17:00 to 17:15, 18:30 to 18:40, 22:30 to 22:40

Table 4. Power ratings (watt) of home appliances across seasons.

Season	AC	WM	EK	VF	LT	MV
Winter	890	500	600	66	36.8	1000
Summer	790	350	600	111	36.8	1000
Autumn	380	450	600	36	36.8	1000
Spring	380	350	600	36	36.8	1000

Table 5. Parameters and scope of the supervisory simulation.

Parameter	Value	Model Role or Limitation
Simulation horizon and interval	24 h; $T_s = 1$ h	Hourly supervisory update consistent with the reported plots
Generation units	One PV and one FC	Recorded seasonal profiles; FC schedule 00:00 to 05:00 and 16:00 to 23:59
Loads	Six household loads	Original demand obtained from Tables 3 and 4; lower-priority loads may be curtailed
ESS count and capacity	$H = 2$; C_{ES_h} = 10,240 Wh each	Equal-capacity configuration of the aggregate energy-balance model
Battery chemistry	Not represented	No electrochemical, temperature, aging, or cycle-life model is used
ESS/bus rated voltage	$V_{dc}^{ref} = 12$ V	Supervisory bus reference used in the aggregate simulation
Initial SoC	ES1: 45%; ES2: 61%	Confirmed against the displayed seasonal profiles
SoC limits	20% to 80%	Confirmed against the displayed seasonal profiles
Charge/discharge efficiency	$\eta_c = \eta_d = 0.92$	Constant aggregate efficiency for both units
ESS power range	1.5 kW per unit	Charging and discharging limit per ESS, consistent with the plotted 0 to 1.5 kW scale
Balancing coefficient	$\gamma_b = 1$	Deadbeat selection at the boundary of the non-alternating range $0 < \gamma_b \leq 1$
Voltage guard	$\Delta V_{guard} = 0.5$ V	Supervisory safeguard threshold on the bus reference
Converter model	Averaged bidirectional interface	Switching frequency, filter values, current-loop gains, and semiconductor losses are not represented
Command-ramp limit	300 W per interval	Applied to the balancing correction at each supervisory update

8. Results and Discussion

This section reports the simulation outcomes of OEMSS under four operating profiles. Summer, winter, autumn, and spring traces are considered to assess the behavior of the supervisory allocation rule under fluctuating renewable generation and household demand.

Figures 4 and 5 compare the SoC trajectories obtained with DDPA and OEMSS for the summer profile, respectively. The corresponding winter results are presented in Figures 6 and 7, followed by the spring results in Figures 8 and 9 and the autumn results in Figures 10 and 11. In each seasonal case, the DDPA results show a persistent difference between the SoC values of the two ESS units because their charging and discharging powers are not adjusted according to the fleet-average SoC deviation. Consequently, one ESS approaches an operational boundary earlier than the other, resulting in unequal storage utilization.

When OEMSS is applied, the charging and discharging contributions of the two ESS units are redistributed according to their individual SoC deviations. The ESS with the higher SoC provides a larger contribution during discharging and receives a smaller

contribution during charging, while the lower-SoC ESS follows the opposite behavior. As a result, the two SoC trajectories approach one another within approximately 2 h for summer and winter and 4 h for spring and autumn. The maximum observed SoC deviation is reduced from 18% under DDPA to 4.8% with OEMSS. These results demonstrate that the supervisory allocation rule reduces SoC divergence in the evaluated two-ESS simulation. However, battery aging, cell health, capacity degradation, and lifetime improvement were not directly evaluated and are therefore not inferred from these results.

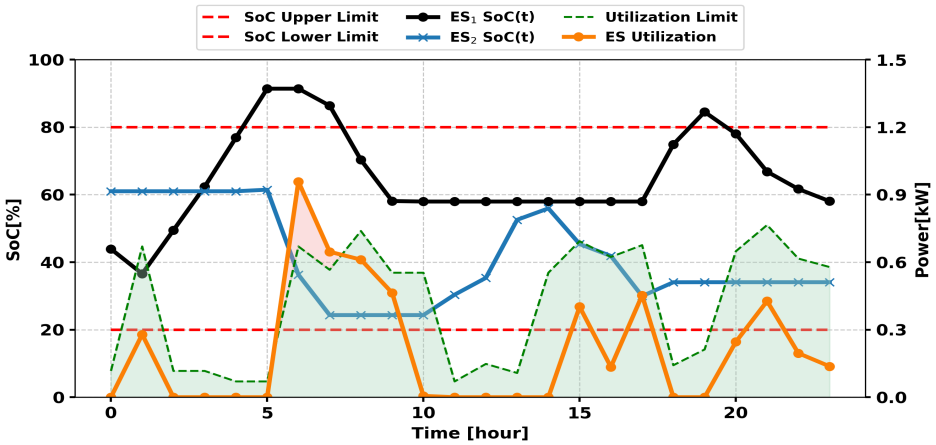


Figure 4. SoC trajectories without supervisory balancing for summer with DDPA.

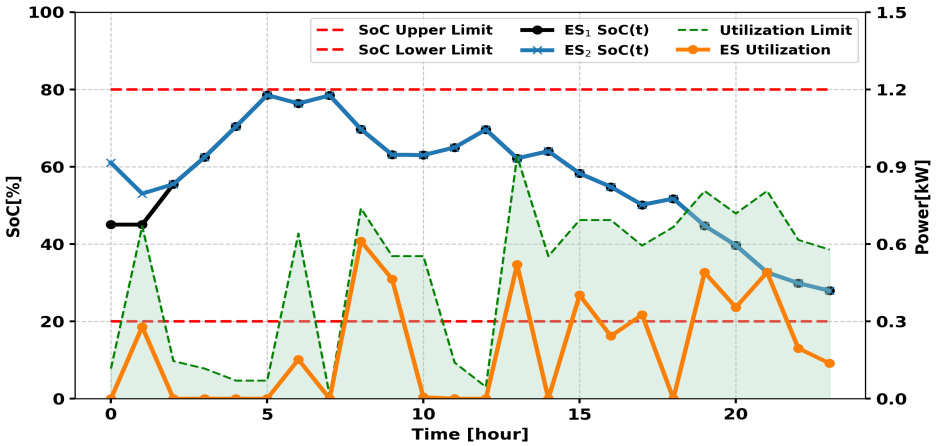


Figure 5. SoC trajectories coordinated within the modeled operating limits for summer with OEMSS.

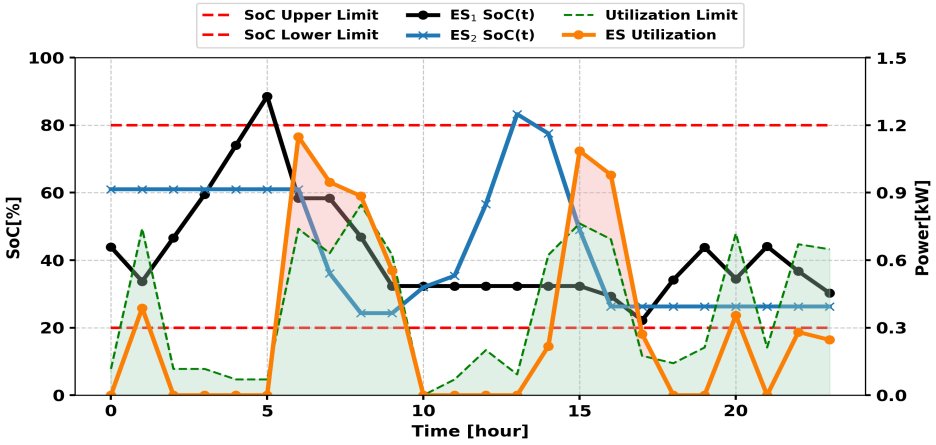


Figure 6. SoC trajectories without supervisory balancing for winter with DDPA.

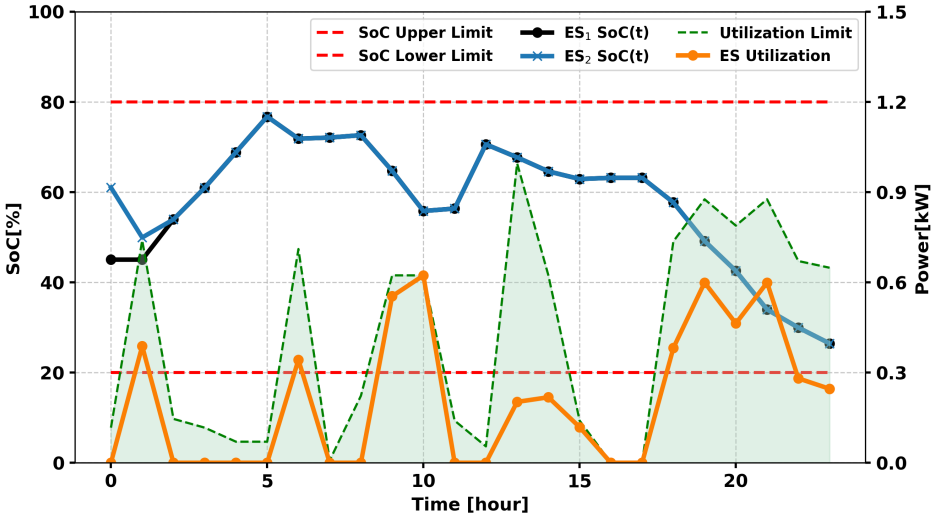


Figure 7. SoC trajectories coordinated within the modeled operating limits for winter with OEMSS.

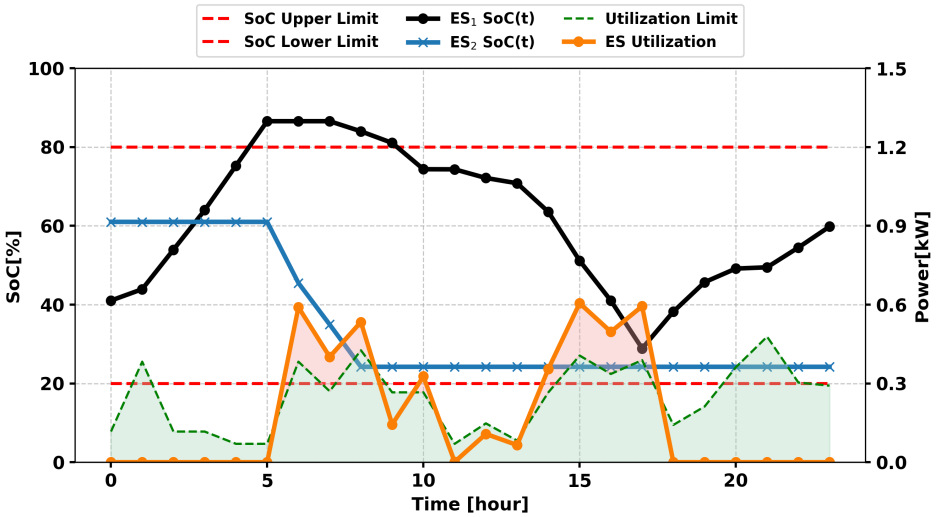


Figure 8. SoC trajectories without supervisory balancing for spring with DDPA.

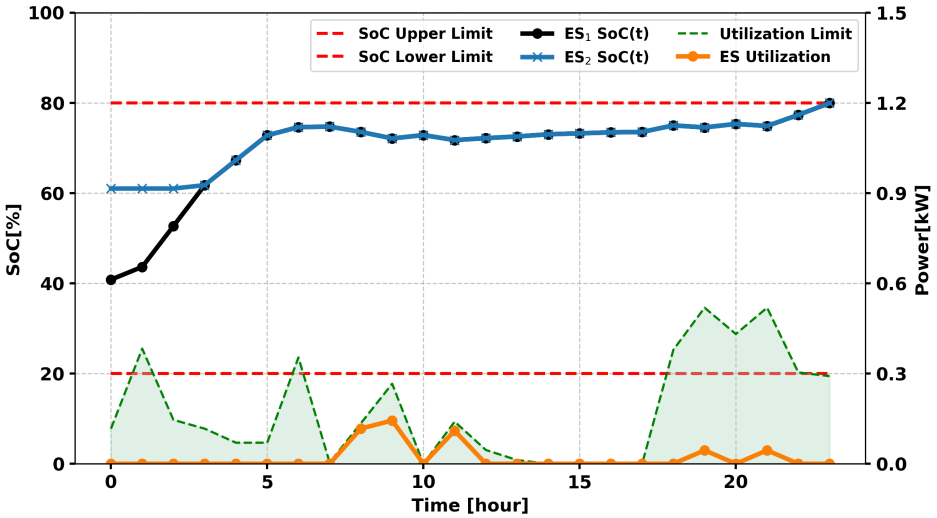


Figure 9. SoC trajectories coordinated within the modeled operating limits for spring with OEMSS.

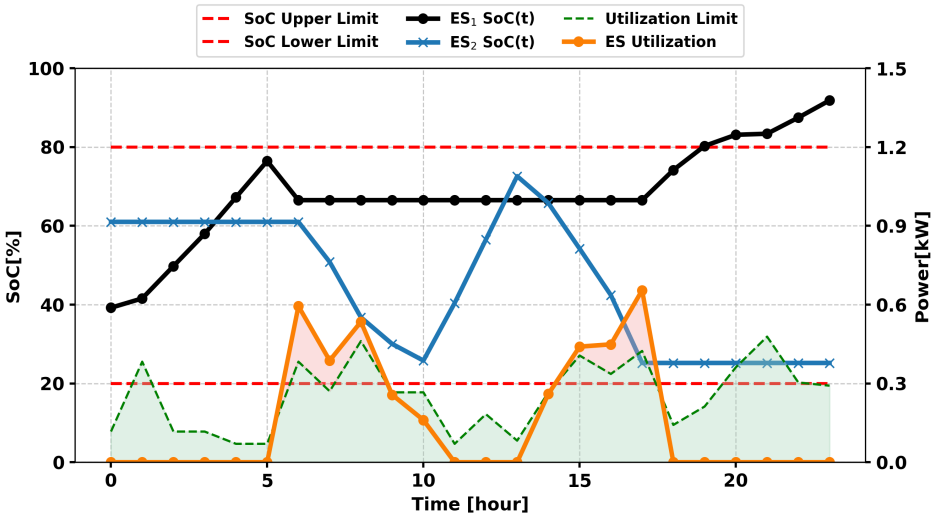


Figure 10. SoC trajectories without supervisory balancing for autumn with DDPA.

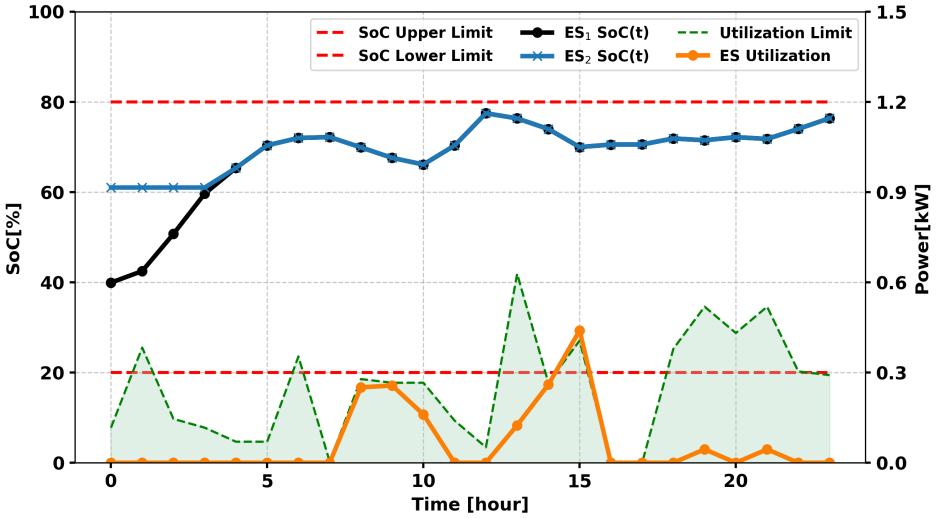


Figure 11. SoC trajectories coordinated within the modeled operating limits for autumn with OEMSS.

The convergence trend is consistent with Section 5.1. For the implemented coefficient $\gamma_b = 1$, which lies in the non-alternating range $0 < \gamma_b \leq 1$, the nominal unsaturated model contracts the SoC deviation vector by the factor $|1 - \gamma_b|$ per supervisory update. The reported outcomes were reproduced by rerunning the simulation with the revised formulation and the parameters of Table 5. The analytical result is not a converter-level voltage-stability proof and does not cover prolonged simultaneous saturation of multiple ESS commands.

The quantity shown in Figures 12–15 is interpreted as storage contribution. The increase from 45% under the baseline representation to approximately 70% with coordinated operation is a 25-percentage-point increase in the ratio of cumulative ESS discharge to cumulative original demand. It is not an increase in round-trip or conversion efficiency and is not sufficient evidence of longer battery life.

Load scheduling is controlled by DDPA in both comparison cases and is not presented as an independent advantage of OEMSS. When the feasible supply is sufficient, the original aggregate demand is served. When priority scheduling is activated, the retained priority demand is supplied and the disconnected low-priority portion contributes to E_{curt} in Equation (25). Accordingly, complete satisfaction of the original aggregate demand is not claimed. A per-interval curtailment log is not available for the reported runs, so no percentage for original-demand service is stated.

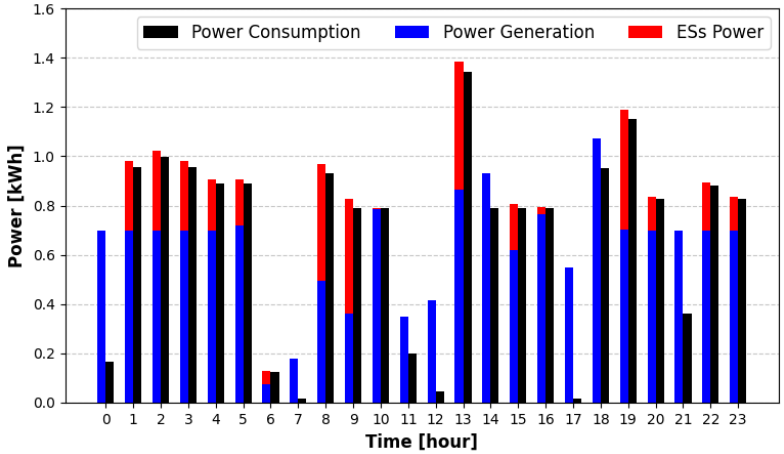


Figure 12. Summer power profiles showing RES generation, load consumption, and ESS contribution under OEMSS; the black bars represent the demand trace used after scheduling.

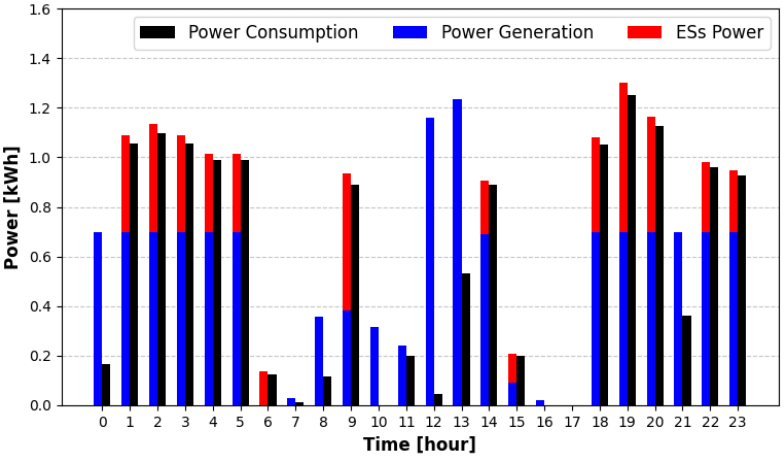


Figure 13. Winter power profiles showing RES generation, load consumption, and ESS contribution under OEMSS; the black bars represent the demand trace used after scheduling.

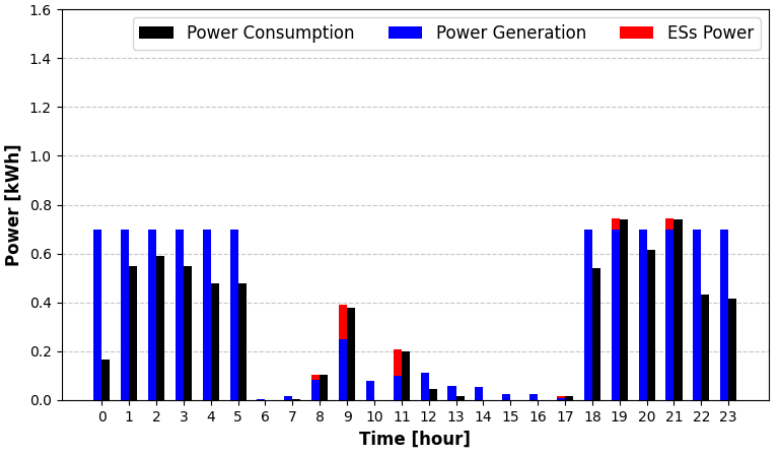


Figure 14. Spring power profiles showing RES generation, load consumption, and ESS contribution under OEMSS; the black bars represent the demand trace used after scheduling.

Table 6 therefore separates verified simulation outcomes from quantities that are not demonstrated. The simulated bus-voltage row refers only to the aggregate model and is not evidence of hardware voltage regulation. Similarly, avoided over-discharge refers to the modeled SoC constraints, not to an experimental battery-protection test.

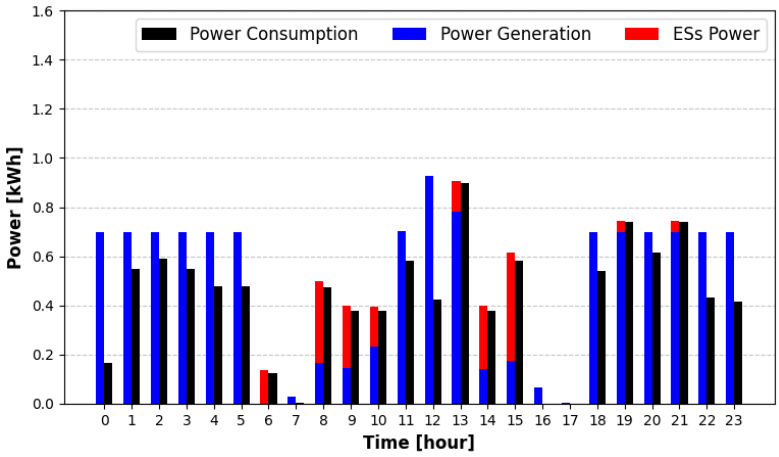


Figure 15. Autumn power profiles showing RES generation, load consumption, and ESS contribution under OEMSS; the black bars represent the demand trace used after scheduling.

Table 6. Verified simulation outcomes and interpretation.

Metric	DDPA Only	DDPA + OEMSS	Permitted Interpretation
Maximum SoC deviation	18%	4.8%	Reduced SoC divergence in the tested two-ESS simulation
Storage contribution rate, ESS_{UR}	45%	Approximately 70%	Increase of 25 percentage points; not conversion efficiency
Simulated DC-bus deviation	12 V $\pm$ 1.2 V	12 V $\pm$ 0.3 V	Aggregate-model observation; no converter-level or hardware validation
Modeled over-discharge events	Present	Avoided	Constraint satisfaction in simulation only
SoC synchronization time	Not achieved	Approximately 2 to 4 h	Seasonal-profile-dependent supervisory convergence
Original aggregate demand	May be curtailed during shortage	May be curtailed during shortage	No claim of complete original-demand satisfaction
Retained priority demand	Supplied after DDPA scheduling	Supplied after DDPA scheduling	Priority-service statement is distinct from original-demand service
Battery life, scalability, and physical efficiency	Not measured	Not measured	Anticipated benefits requiring dedicated experiments

9. Conclusions

This study evaluated a supervisory SoC redistribution rule integrated with Demand-Driven Power Allocation for a simulated DC microgrid containing two generation sources, two equal-capacity ESS units, and six household loads. In the four seasonal profiles, adding OEMSS to DDPA reduced the maximum SoC deviation from 18% to 4.8% and produced approximate synchronization within 2 to 4 h. The modeled SoC constraints prevented over-discharge events in the reported runs. The ratio of cumulative ESS discharge to cumulative original demand increased from 45% to approximately 70%, which is reported as a 25-percentage-point increase in storage contribution and not as an efficiency improvement.

The charging and discharging allocation laws were separated and written with the dimensionally consistent factor C_{ES_h}/T_s. For the unsaturated supervisory model, the Lyapunov analysis gives $0 < \gamma_b < 2$, while $0 < \gamma_b \leq 1$ yields non-alternating decay. The online update remains linear in the numbers of generators, loads, and ESS units. These results

support the limited conclusion that a simple average-SoC-based redistribution rule can reduce SoC divergence when combined with DDPA in the tested simulation.

Several claims remain unproven by the evidence.The study does not establish global optimality, chemistry-specific battery-life extension, conversion-efficiency improvement, hardware scalability, or converter-level voltage stability. Priority scheduling may fully supply the retained priority demand while curtailing part of the original demand; therefore, complete original-demand satisfaction is not claimed. Future work will preserve interval-level original-demand, served-demand, and curtailed-energy logs and will evaluate unequal ESS capacities. Hardware-in-the-loop testing will then measure converter dynamics, DC-bus transients, execution time, communication delay, sensor noise, saturation behavior, and battery-model sensitivity before practical deployment claims are made.

Author Contributions: Conceptualization, M.S., S.J., and Y.L.; methodology, M.S., S.J., and I.I.I.; software, M.S. and I.I.I.; validation, S.J. and I.I.I.; formal analysis, S.J. and I.I.I.; writing—original draft preparation, M.S.; writing—review and editing, M.S., S.J., I.I.I., and Y.L.; supervision, S.J., Y.L., and Y.T. All authors have read and agreed to the published version of the manuscript.

Funding: This research received no external funding.

Data Availability Statement: The original contributions presented in the study are included in the article; further inquiries can be directed to the corresponding author.

Acknowledgments: The authors have reviewed and edited the output and take full responsibility for the content of this publication.

Conflicts of Interest: The authors declare no conflicts of interest.

Abbreviations

The following abbreviations are used in this manuscript:

Abbreviations	
AC	Air Conditioner
AES	All-Electric Ship
BM3	Battery Modular Multilevel Management
BESS	Battery Energy Storage System
DBS	DC Bus Signaling
DC	Direct Current
DER	Distributed Energy Resources
DESU	Distributed Energy Storage Unit
DPN	Distributed Power Network
DSCC	Double-Star Chopper Cell
EG	Energy Generator
EGs	Energy Generators
EL	Energy Load
ELs	Energy Loads
ESS	Energy Storage System
ESSUR	Legacy symbol for the ESS storage contribution rate
EV	Electric Vehicle
FC	Fuel Cell
HAD	Home Appliances and Devices
MG	Microgrid
MMC	Modular Multilevel Converter
OEMSS	Energy-Management and SoC Balancing Scheme
PCS	Power Conditioning System
PL	Power Load
PV	Photovoltaic

RES	Renewable Energy Sources
RER	Renewable Energy Resources
RL	Reinforcement Learning
SEMS	Smart Energy Management System
SoC	State of Charge
VDCM	Virtual DC Motor
VF	Ventilation Fan
WM	Washing Machine
LT	Light
EK	Electric Kettle
MV	Microwave Oven
Nomenclature	
t	Time index
j	Index of energy generators, $j \in \{1, 2, \ldots, J\}$
k	Index of energy loads, $k \in \{1, 2, \ldots, K\}$
h	Index of energy storage systems, $h \in \{1, 2, \ldots, H\}$
$EG_j(t)$	Power generated by the j-th energy generator at time t
$EL_k(t)$	Power demand of the k-th energy load at time t
$\mathcal{E}_{\mathrm{EG}}(t)$	Total generated energy from all EGs
$\mathcal{E}_{\mathrm{EL}}(t)$	Total consumed energy by all ELs
$\mathcal{E}_{\mathrm{ES}_h}(t)$	Stored energy of the h-th ESS
$\mathcal{E}_{ES_h}^{ini}$	Initial energy of the h-th ESS
$\mathcal{E}_{ES_h}^{in}(t)$	Charging energy of the h-th ESS
$\mathcal{E}_{ES_h}^{out}(t)$	Discharging energy of the h-th ESS
C_{ES_h}	Rated energy capacity of the h-th ESS
$P_{ES_h}^{in}(t)$	Charging power of the h-th ESS
$P_{ES_h}^{out}(t)$	Discharging power of the h-th ESS
$P_{ES_h}^{min}$	Minimum allowable ESS power
$P_{ES_h}^{max}$	Maximum allowable ESS power
$SoC_h(t)$	State of charge of the h-th ESS at time t
SoC_h^{ini}	Initial state of charge of the h-th ESS
SoC_h^{min}	Minimum allowable SoC of the h-th ESS
SoC_h^{max}	Maximum allowable SoC of the h-th ESS
ΔSoC_h	Deviation of SoC of ESS-h from the capacity-weighted average SoC
$\overline{SoC}_C$	Capacity-weighted average state of charge
γ_b	Dimensionless supervisory SoC balancing coefficient
T_s	Energy-management sampling interval
V_{dc}	Measured DC-bus voltage
V_{dc}^{ref}	DC-bus voltage reference
ΔV_{guard}	DC-bus voltage guard band
P_{ES}^{in}	Fleet charging request
P_{ES}^{out}	Fleet discharging request
P_L^{orig}	Original aggregate load demand before priority scheduling
P_L^{srv}	Served or retained load demand after priority scheduling
e_h	SoC deviation of ESS-h from the capacity-weighted average
α_h	Capacity share of ESS-h
$Ratio_{ES_h}^{c}$	Charging ratio of ESS-h
$Ratio_{ES_h}^{d}$	Discharging ratio of ESS-h
η_c	Charging efficiency of ESS
η_d	Discharging efficiency of ESS
E_{loss}	Total energy loss in the system
ESS_{UR}	ESS storage contribution rate retained as a legacy symbol
DSR	Original-demand service ratio

E_{curt}	Energy curtailed through priority scheduling

References

1. Shaukat, N.; Islam, M.R.; Rahman, M.M.; Khan, B.; Ullah, B.; Ali, S.M.; Fekih, A. Decentralized, Democratized, and Decarbonized Future Electric Power Distribution Grids: A Survey on the Paradigm Shift From the Conventional Power System to Micro Grid Structures. *IEEE Access* **2023**, *11*, 60957–60987. [CrossRef]
2. Yao, D.; Cui, K.; Li, H.; Yang, C.; Liu, B. Power Flow Calculation of Shipboard DC Microgrid Power System. In Proceedings of the 2019 IEEE Third International Conference on DC Microgrids (ICDCM), Matsue, Japan, 20–23 May 2019; pp. 1–6. [CrossRef]
3. Al-Ismail, F.S. A Critical Review on DC Microgrids Voltage Control and Power Management. *IEEE Access* **2024**, *12*, 30345–30361. [CrossRef]
4. Elsayed, A.T.; Mohamed, A.A.; Mohammed, O.A. DC microgrids and distribution systems: An overview. *Electr. Power Syst. Res.* **2015**, *119*, 407–417. [CrossRef]
5. Garg, A.; Tummuru, N.R.; Oruganti, R. Implementation of Energy Management Scenarios in a DC MG Using DC Bus Signaling. *IEEE Trans. Ind. Appl.* **2021**, *57*, 5306–5317. [CrossRef]
6. Barone, G.; Brusco, G.; Menniti, D.; Pinnarelli, A.; Sorrentino, N.; Vizza, P.; Burgio, A.; Bayod-Rújula, Á. A Renewable Energy Community of DC Nanogrids for Providing Balancing Services. *Energies* **2021**, *14*, 7261. [CrossRef]
7. Zhang, L.; Wu, T.; Xing, Y.; Sun, K.; Gurrero, J.M. Power control of DC microgrid using DC bus signaling. In *Proceedings of the 2011 Twenty-Sixth Annual IEEE Applied Power Electronics Conference and Exposition (APEC)*; IEEE: Piscataway, NJ, USA, 2011; pp. 1926–1932.
8. Lee, C.; Kwon, H.; Lee, Y.I. OPC UA-based three-layer architecture for aggregated microgrids integrating edge cloud computing and IEC 62264. *J. Ind. Inf. Integr.* **2025**, *48*, 100965. [CrossRef]
9. Panda, M.; Devara, V.B.; Maity, T. A novel dc bus-signaling based power management strategy for dc microgrid. *Int. Trans. Electr. Energy Syst.* **2021**, *31*, e12758.
10. Chen, S.; Lu, X.; Gong, Q. SOC Balance and Economic Dispatch Using Distributed Cooperative Control for Distributed Energy Storage systems in DC Microgrid Applications. In Proceedings of the IECON 2020 The 46th Annual Conference of the IEEE Industrial Electronics Society, Singapore, 18–21 October 2020; pp. 3371–3376. [CrossRef]
11. Javaid, S.; Lim, Y.; Tan, Y.; Ioannou, I.I. Safety Based Optimal Storage Capacity Sizing for Power System with Renewable Energy Sources. In Proceedings of the 2024 20th International Conference on Distributed Computing in Smart Systems and the Internet of Things (DCOSS-IoT), Abu Dhabi, United Arab Emirates, 29 April–1 May 2024; pp. 462–468. [CrossRef]
12. Fonseca, J.M.L.; Reddy, S.R.P.; Rajashekara, K.; Raj, K. Active Power and SOC Balancing Techniques for Resilient Battery Energy Storage Systems under Asymmetric Grid Voltage Scenarios. In Proceedings of the 2021 IEEE Applied Power Electronics Conference and Exposition (APEC), Phoenix, AZ, USA, 14–17 June 2021; pp. 947–954. [CrossRef]
13. Qi, L.; Wang, A.; Guo, S.; Sun, X.; Wang, P. State of Charge Balancing Control for DESUs in PV Battery based AC Nanogrid. In Proceedings of the 2018 IEEE International Power Electronics and Application Conference and Exposition (PEAC), Shenzhen, China, 4–7 November 2018; pp. 1–5. [CrossRef]
14. Al-Taie, R.R.; Hesselbach, X. Cost-Effective Power Management for Smart Homes: Innovative Scheduling Techniques and Integrating Battery Optimization in 6G Networks. *Electronics* **2024**, *13*, 4231. [CrossRef]
15. Fagundes, T.A.; Fuzato, G.H.F.; Silva, L.J.R.; dos Santos Alonso, A.M.; Vasquez, J.C.; Guerrero, J.M.; Machado, R.Q. Battery energy storage systems in microgrids: A review of SoC balancing and perspectives. *IEEE Open J. Ind. Electron. Soc.* **2024**, *5*, 961–992. [CrossRef]
16. Thurlbeck, A.P.; Siddiquee, A.; Kisacikoglu, M.J.; Sozer, Y. Active SOC Balancing for a Multi-Chemistry Battery Pack with Reduced Number of Converters. In Proceedings of the 2023 IEEE Energy Conversion Congress and Exposition (ECCE), Nashville, TN, USA, 29 October–2 November 2023; pp. 1895–1902. [CrossRef]
17. Guo, Y.; Song, S.; Guan, C. A Distributed SOC Balance Control Strategy in the DC Microgrid Based on the Virtual DC Machine Control. In Proceedings of the 2024 IEEE 7th International Conference on Information Systems and Computer Aided Education (ICISCAE), Dalian, China, 27–29 September 2024; pp. 925–930. [CrossRef]
18. Karnehm, D.; Pohlmann, S.; Neve, A. State-of-Charge (SoC) Balancing of Battery Modular Multilevel Management (BM3) Converter using Q-Learning. In Proceedings of the 2023 IEEE Green Technologies Conference (GreenTech), Denver, CO, USA, 19–21 April 2023; pp. 107–111. [CrossRef]
19. Mostafa, A.; Gaafar, M.A.; Abdel-Rahim, O.; Orabi, M. Comparative Study of the State of Charge (SoC) Balancing Techniques for Battery Power Module Configurations. In Proceedings of the 2023 IEEE Conference on Power Electronics and Renewable Energy (CPERE), Luxor, Egypt, 15–17 February 2023; pp. 1–5. [CrossRef]
20. Wu, S.; Zhou, J.; Zhang, Y.; Feng, Y. Integrated Learning Based SOC Balancing Control Method for Electric Vehicle Charging Stations. In Proceedings of the 2024 4th International Conference on Computer Science and Blockchain (CCSB), Shenzhen, China, 6–8 September 2024; pp. 57–60. [CrossRef]

21. Qi, X.; Gao, H.; Peng, F.; Luo, R.; Ma, W. Distributed Energy Storage SOC Balancing Strategy Based on Adaptive Droop Control with Dynamic Correction Coefficients. In Proceedings of the 2024 5th International Conference on Mechatronics Technology and Intelligent Manufacturing (ICMTIM), Nanjing, China, 26–28 April 2024; pp. 810–813. [CrossRef]
22. Deng, Y.; Sun, C.; Qiu, S.; Li, Y.; Sui, C.; Han, W. SOC Balancing Control Strategy of DC Microgrid Energy Storage System Based on Droop Control. In Proceedings of the 2023 International Conference on Power System Technology (PowerCon), Jinan, China, 21–22 September 2023; pp. 1–5. [CrossRef]
23. Ye, X.; Jia, Y.; Zhang, J.; Zhang, W.; Yang, C.; Jiang, D. SoC Balancing Strategy of Multi Energy Storage System in Islanded Microgrids Considering Acceleration Factor Setting. In Proceedings of the 2023 8th Asia Conference on Power and Electrical Engineering (ACPEE), Tianjin, China, 14–16 April 2023; pp. 2603–2608. [CrossRef]
24. Muhammad, S.; Javaid, S.; Ioannou, I.; Lim, Y.; Tan, Y. Mitigating Energy Losses Under Incremental Load Variations in Distributed Power-Flow Systems While Ensuring User Comfort. *Energies* **2025**, *18*, 5716. [CrossRef]

Disclaimer/Publisher's Note: The statements, opinions and data contained in all publications are solely those of the individual author(s) and contributor(s) and not of MDPI and/or the editor(s). MDPI and/or the editor(s) disclaim responsibility for any injury to people or property resulting from any ideas, methods, instructions or products referred to in the content.